Characterization of Magnetic Communication Through Human Body

Rajpreet K Gulati[1], Sayemul Islam[2], Amitangshu Pal[1], Krishna Kant[1], Albert Kim[2]

***Abstract*—Biomedical systems of implanted miniaturized sensors and actuators interconnected into an intra-body area network could revolutionize treatment options for chronic diseases afflicting internal organs. Given the well-understood limitations of radio frequency (RF) propagation in the human body, we have explored magnetic resonance (MR) coupling for both communications and energy transfer through the body. In this paper, we discuss the design and implementation of a software-defined prototype using USRP boards. We report experimental results on the power received and achieved packet error rates at different through-the-body distances and packet sizes. We show that the MR signal propagates through the body substantially better than in the air, and can provide a practical means for energy transfer and communications in intra-body networks. We also show that it works better than the better understood galvanic coupling.**

***Index Terms*—Magnetic resonance coupling; magnetic communication; intra-body sensor network; wireless power transfer;**

I. Introduction

With an aging population in most countries and increasing pollution, chronic diseases are becoming quite common. For example, in the US, approximately 45%, or 133 million, people suffer from at least one chronic disease [1] and more than 50% of older adults suffer from $\geq$ 3 chronic conditions [2]. Many of these can be actively managed using implantable medical devices (IMDs) [3], [4]. IMDs have made significant improvements in recent years, with advancements in integrated circuits, MEMS, wireless systems, and battery technologies. IMDs have two related functions: (a) to measure disease-related parameters and control the delivery of drugs or physiological stimuli (e.g., electric shock), and (b) to perform physiological health monitoring such as implanted cardio-defibrillators, implantable neuro-stimulators, etc. to assist physicians in providing advice to the patient regarding a change in type or quantity of medications, avoiding certain foods, avoiding a certain type of movements, etc.

In some chronic diseases or natural function defects of organs, the formation of a therapeutic network of multiple sensors and actuators in the body can achieve unprecedented management, such as a spinal neuro-modulator based on bladder pressure monitoring to control overactive bladder through implanted pressure sensor and micro-electrode mediated nerve recording to monitor urine output [5]–[7]; effectively control the pacemaker through monitoring of pH, oxygen, respiration, activity and drug infusion [8], [9]; or through a brain-computer interface via implantable microelectrode arrays (where the number of channels can exceed 100) [10].

All these applications require robust and highly energy-efficient means of *Human Body Communication* (HBC), i.e., communication between intra-body nodes (or on body nodes entirely through the body media). The limitations of radio frequency (RF) communications for HBC are well known [11], [12], and several alternative technologies have been proposed, but their relative merits in terms of data transfer are not very clear. Exploring this aspect experimentally forms the key contribution of this paper.

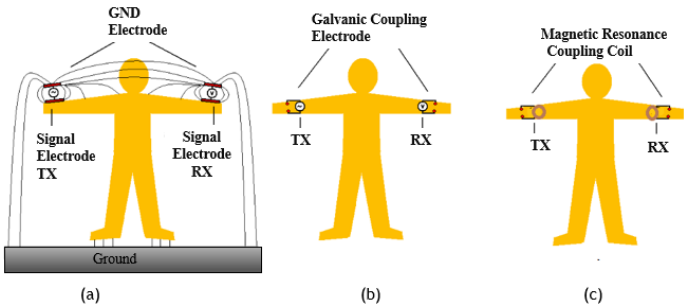

Fig. 1. Intra-body coupling methods: (a) galvanic coupling, (b) capacitive coupling, and (c) magnetic resonance (MR) coupling.

The HBC signal propagation methods can be classified as galvanic coupling (GC) [13], [14], capacitive coupling (CC) [15], [16], and magnetic resonance coupling (MR) [17]–[19]. Fig. 1 briefly illustrates their working principle.

Galvanic HBC couples the signal to the human body through a pair of electrodes in contact with the skin that serves as a transmitter (T_x) and receiver (R_x) respectively. This is shown in the figure 1(a) with the two electrode pairs on the wrists. The human body has a relatively low conductivity, so the signal flowing between the transmit and receive electrodes is rather small [20]. Instead, due to very short spacing between the positive and negative terminals on each end, much of the current flows locally. Thus GC coupling does not provide a very efficient way of energy transfer or communication across the body. The GC signal frequency ranges from as low as 10 kHz to 100 MHz for most effective communication. Recent work has shown data rates up to 1.23 Mbps when transmitting at 200 kHz with attenuation levels typically around 50 dB over a distance of 15 cm [21].

The capacitive coupling (also known as electrostatic coupling) uses T_x and R_x electrodes as shown in figure 1(b). The signal electrodes are capacitively attached to the body while the ground electrodes are left floating, creating a ca-

[1]Department of Computer and Information Sciences, [2]Department of Electrical and Computer Engineering, Temple University, Philadelphia, Pennsylvania 19122 USA.

pacitance with the environment (earth, air, or other objects in the surrounding). Capacitive coupling can be modeled as a distributed RC circuit [22]. Recent work on capacitive coupling at 60 MHz exhibits an attenuation of 20-25 dB and covers a 140 cm body distance. Due to the weak nature of the signal transmission and being highly affected due to the surrounding environment, the capacitive coupling technique in HBC is typically effective over a shorter range [23] [16], making it inefficient and unsuitable for using with wearable and implantable devices at longer link distance.

The magnetic resonance coupling refers to the signal coupling between the T_x and R_x coils via magnetic flux as shown in Fig. 1(c). Both transmitter and receiver consist of an identical inductive coil in parallel with an identical capacitor to form a resonant LC circuit that can transfer energy quite efficiently at the resonance frequency. The spectral range most frequently utilized in MR coupling spans from about 100KHz to 50 MHz yielding a maximum attenuation of only 8.1 dB over a distance of 40 cm covered [21].

Although MR coupling has been studied in the past, there are no comprehensive results for packet loss rate as a function of packet size and in-body distance. The wavelength of the magnetic field suggested in Park's study [21] is 2.3m at 21 MHz in air, which has the potential to interfere with the magnetic fields of other adjacent devices.

In the following, we explore these different technologies experimentally.

II. Experiment Setup

A. Instruments

There are many SDR development platforms [24] [25] that utilize FPGAs or specialized CPUs for high-sample-rate digital signal processing. We chose USRP [24] because of its cheap cost and widespread use in academics and industries. A motherboard and two daughterboards comprise the Universal Software Radio Peripheral (USRP) (USRP N210). The primary processing unit is the motherboard, which includes AD/DA converters (a dual 100 MSPS 14-bit ADC and a dual 400 MSPS 16-bit DAC) and an FPGA unit (Spartan 3A-DSP 3400). The daughterboards are radio frequency (RF) front ends that connect the device to a transmitter or receiving antennas. We utilize LFTX and LFRX daughterboards that run from DC to 30 MHz, which covers frequency ranges that we are interested in.

We used USRP N210 and LFTX and LFRX daughterboard to measure the data rate of the packet received between transmitter and receiver. We also measured power received to determine the signal attenuation of galvanic and magnetic resonance couplings. We connected electrodes (for galvanic) or coils (for MR) to the USRP N210. We used the transmission frequency of 13.57 MHz, which is the most commonly recommended frequency of MR coupling and corresponds to RFID frequency. The transmission power was maintained at 0 dBm (1 mW) throughout the study. The measurement devices were carefully calibrated before each experiment to ensure accurate measurements. Fig 2 shows the transmit/receive antennas for the three coupling methods.

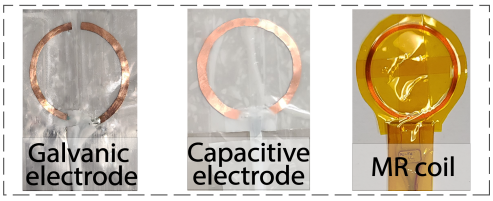

Fig. 2. Transmit (and receive) antennas for different coupling methods

For galvanic coupling, an electrical insulator is inserted in the middle of two half circular conductive copper sheets (width = 1.6 mm, dia = 33.2 mm, thickness = 0.1 mm) as shown in (Fig.2)(a), which serve as our electrodes (T_x and R_x). Bio-compatible polypropylene film based pressure-sensitive adhesive (PSA) tape (ARseal 90880, Adhesives Research) is used to attach galvanic electrodes directly to skin. This increases the conductivity and eliminates air gaps.

For the capacitive coupling experiments, the setup was placed on an insulated platform 10 cm above the ground to create ground coupling through ground capacitance. Two separate copper sheets (10 cm $\times$ 3 cm) were connected to each T_{x-} and R_{x-} (negative) electrode. Each electrode has width = 1.6 mm, dia = 33.2 mm and thickness = 0.1 mm. The subject was also asked to stand on an insulated platform, about 1 cm above the ground. Subject's forearms were attached to the polyimide insulated T_{x+} and R_{x+} electrodes, which created a capacitive coupling with the body as shown in (Fig.2)(b).

For the MR coupling experiments, commercially available RFID coils (Zycoil Electronic Co.) as shown in (Fig.2)(c) coupled with a capacitor as T_x and R_x were used. The inductance (made out of 10 turns of 34 AWG, polyimide insulated copper wire, dia = 33.2 mm) of 9.27 μH is used with the planar coil. It is connected in parallel with a 14.86 pF capacitor, forming an LC circuit with a resonance frequency of 13.56 MHz. Two other hand-wound coil pairs (950 nH, 26 AWG, 2 loops, 48 mm diameter) are used in this study (reported in section III-A).

We measured the received power, which can also be regarded as the received signal strength indicator (RSSI). GNU radio software along with USRP N210 boards were used to measure the received power and the received power was calculated using the formula $P(dBm) = 10 \cdot log_{10}[P(mW)/1mW]$, where $P(mW) = V^2/R$, and R is the resistance of the USRP (1 $M\Omega$). The transmitter and receiver coil were covered by a specialized magnetic shielding film (WMF200, Woremor) to minimize magnetic interference from nearby electronic equipment and over-the-air transmission [26]. While using the magnetic shield at 100 cm range, the power measured was -65 dBm.

B. Packet Transmission Technique

For narrowband transmission, the 13.56 MHz carrier can be digitally modulated by switching signal (on-off keying;

OOK), frequency (frequency shift keying; FSK), or carrier phase (phase shift keying; PSK). The bandwidth of all three technologies is approximately equal to the signaling rate. Phase shift keying is a modulation format widely used in low bit-rate applications with moderate error performance. Due to its simplicity and low hardware cost, BPSK seems ideal. PSK detection typically uses two matched band-pass filters tuned to the carrier frequency and phase shift, as well as a symbol detector and decision circuit. Coherent PSK detection is better when using synchronous detection noise suppression, but must be synchronized with the transmitter's frequency. The best solution focuses on high receiver sensitivity and simplicity at a reasonable data rate.

Understanding the minimum received power required by the transmitter to ensure signal detection at the receiver input is critical in low-power operation. As a result, the transmitter's output power requirement is determined by the following: 1) Electronic system noise, 2) Interface electrode noise, 3) Selected modulation scheme, 4) Channel attenuation, and 5) the receiver input noise figure, N = $4kTR_{input}$. The front end of the receiver has a high gain, low noise amplifier, so it is assumed that it contributes most to the circuit's equivalent input noise. This provides a minimum transmitter output power of 10 dBm for 2 k electrode/tissue load and a 6 V power supply. The ICNRP guidelines limit the maximum output power to 8 dBm.

C. Wireless transmission using USRP and GNU radio

A series of signal processing blocks can be combined to create flow graphs in the GNU Radio project. These blocks are built using C++ or Python programming language, which has several benefits, such as simple installation, connectivity, and the easy generation of GUIs.

Existing GNU Radio blocks span different applications from basic math to sophisticated digital filters, modulators/demodulators, channel codecs, voice codecs, etc. Input/output blocks are a subclass of blocks. They provide a connection to the actual world; the most well-known of them is the UHD (USRP hardware driver). The UHD blocks are designed to make use of the USRP and transmit/receive signals via a wireless channel.

The detailed block diagram of GNU radio is shown in Fig. 3. In the transmitter, the block vector source sends a vector (a string of bits) by the user. The output of the vector source is connected to the packet encoder which is responsible for encoding the data. After the encoder, the encoding data are sent to the PSK modulator. The PSK modulator was configured as a BPSK modulator. The signal from the BPSK modulator is sent to the USRP Sink block which is responsible for interacting with the USRP. This block has several parameters that are used by the hardware, such as, center frequency and the antenna type used on the daughter-board. Then, connect the coils with SMA cables and connectors both transmitter (TX) and receiver(RX). It creates magnetic induction between TX and RX. The USRP Source output is connected to the PSK Demod block that demodulates the PSK signal (BPSK in this example), recovering the encoding data. After the demodulation, the encoding data is sent to the packet decoder block, which decodes the data and outputs the bits (the information sent by Vector Source). Then, convert the data into bytes.

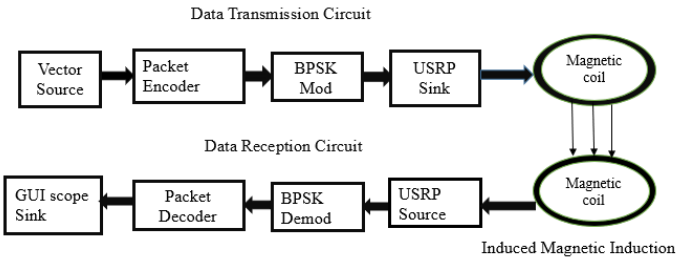

Fig. 3. Block diagram of Wireless transmission with USRP board and GNU radio

D. Experimental protocol with human subjects

Except for some air experiments, all experiments in this study were conducted on the human body. The experimental methods were approved by the department IRB and regulatory affairs. We conducted RSSI experiments with several volunteers of different ages, body builds, and gender. These results may be found in [27] and are not included here, since our focus in this paper is on packet delivery issues that are not studied in [27]. We found that person-to-person variations are quite small in all cases; therefore, all packet transmission experiments conducted for this paper are for a single volunteer. We also found that the body movement or different poses do not have much impact on the signal strength, and are thus not expected to affect packet delivery. Therefore, the results reported here are for a volunteer in a standing position as discussed earlier.

The position used was with the arms extended to the sides of the body horizontally. The arms were straight. The transmitter was placed on the left hand. The receiver was placed at a distance of 5*N cms from the position of the transmitter on the left hand, where N = 1,2,... In successive experiments, the receiver is moved towards the right hand, over the arms. The overall range of variation of the receiver was 125 cms. In another configuration that we used, the transmitter was placed on the shoulder, and the receiver was moved in steps of 5 cms down towards the feet on the body.

In a single run, 1000 packets were sent from the transmitter to the receiver. The frame structure of the packets is explained in section II-E. The results from both of these setups are similar w.r.t distance from the transmitter and skin tissue. They are listed in table I. The percentage difference of both configurations in terms of the packet received lies between 0 to 0.2. The measurements were taken with the subject standing on a ground isolated platform in our lab.

E. Frame Structure

We used the packet frame structure shown in Fig. 4 to send the data packets between transmitter and receiver. The

TABLE I
CHANGE IN THE CONFIGURATION OF PLACEMENT OF RECEIVER COIL (TRANSMITTING PACKETS (T) ARE 1000)

Distance	Left hand to right hand(A)	Shoulder to feet (B)	% difference, D=|B-A|×100 / T
30cm	1000	1000	0
60cm	1000	1000	0
90cm	750	752	0.2
120cm	20	19	0.1

minimum packet size used was 56B.

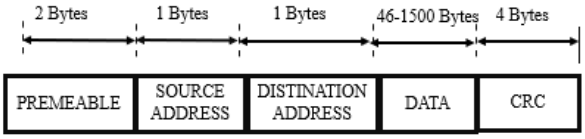

Fig. 4. Frame Structure

- Preamble - This is a 2-Byte field. It indicates starting of the frame and allows sender and receiver to establish bit synchronization.
- Source Address – This is a 1-Byte field that contains the address of the source node. (256 possible nodes in an intra-body network is plenty).
- Destination Address – This is a 1-Byte field that contains the address of a node for which data is destined.
- Data Payload. The maximum data present may be as long as 1500 Bytes.
- Cyclic Redundancy Check (CRC) – This is standard 32-bit CRC. If the CRC computed by destination is not the same as the sent CRC value, the data received is considered to be corrupted.

By a careful comparison between sent and received data, we found that in all cases, the CRC was able to detect the error; therefore, all packets received without the CRC error represent packets that do not suffer from any bit flips.

F. Safety considerations

Unregulated, non-static electromagnetic fields may cause adverse health effects on humans [28] especially when under long term exposure. In this paper, we strictly maintain the power transmission power output of the USRP boards at 0 $dBm(1\ mW)$. For 13.56 MHz frequency, we maintain the magnetic flux density much lower than the safety recommendation by IEEE standards. Our magnetic flux density is maintained less than 1 μT (table: II).

III. RESULTS AND DISCUSSION

A. Performance comparison using different MR coils

We investigated how the coil design affects the signal transmission performance. Considering the magnetic flux density, inductance, and mutual coupling factors, We selected three different MR coils henceforth called coils A, B, and C respectively. (Fig. 5(a-c)). For this experiment, we set the resonance frequency for all coils at 13.56 MHz.

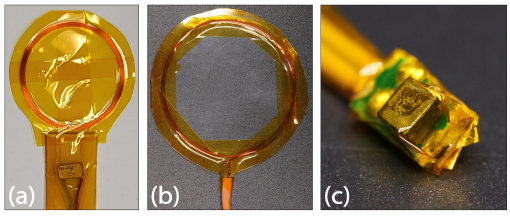

Fig. 5. Three MR coil performance compared: (a) coil - 33.2 mm, (b) coil -

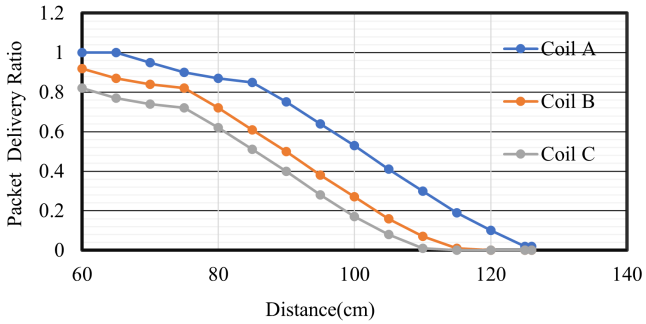

Fig. 6. Distance versus packet delivery ratio with three MR coil performance

Table II shows the design specifications for these coils. As before, matched T_x and R_x coils were placed in the forearms of a human subject and covered by the magnetic shielding films as shown in Fig. 7(a). Fig. 6 shows the relationship between the number of data packets received correctly and the distance from the source with three different coils. The experimental results show that the MR coil A, which has the biggest overall size (33.2 mm diameter and 10 turns) resulted in the best transmission performance. It received 100% packets at 65 cm and 50% at 100 cm. Coil B, which has 48 mm diameter but only 2 turns, shows worse behavior, and Coil C is the worst (50% packets received at 85 cm). This is not surprising since coil A generates the highest magnetic flux, and coil C the smallest. Coil A performs comparatively better performance. We have used this design in other experiments.

TABLE II
MR COIL SPECIFICATIONS (RESONANCE FREQUENCY = 13.56 MHZ)

Parameter	Coil A	Coil B	Coil C
1. Dimension	Dia = 33.2 mm N = 10 turns	Dia = 48 mm N = 2 turns	L = 3.2 mm W = 2.0 mm
2. Inductance	9.27 μH	950 nH	15 nH
3. Capacitance	14.86 pF	145 pF	9.2 nF
4. Magnetic flux density	0.962 ± 0.01 μT	0.224 ± 0.001 μT	0.074 ± 0.004 μT

B. MR coupling vs. other coupling methods

Figure 7 illustrates the relationship between the packet delivery ratio (PDR) and the distance from the source. The figure shows both MR and galvanic coupling results through the body; for comparison, the results on MR transmission through the air are also shown. The body forms a much better transmission media than Air, with MR providing a much higher range than Air. It is also seen that the MR transmission is significantly better than galvanic; as stated earlier, this is

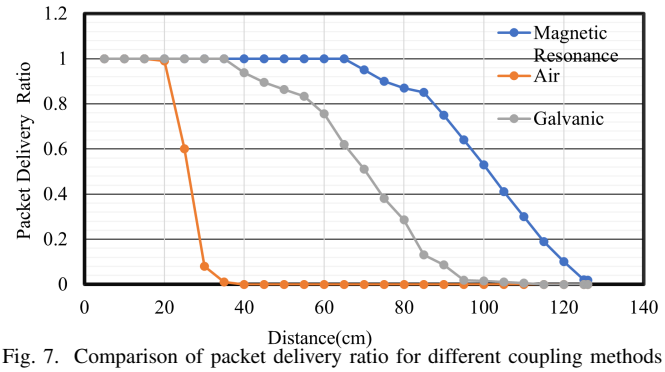

Fig. 7. Comparison of packet delivery ratio for different coupling methods

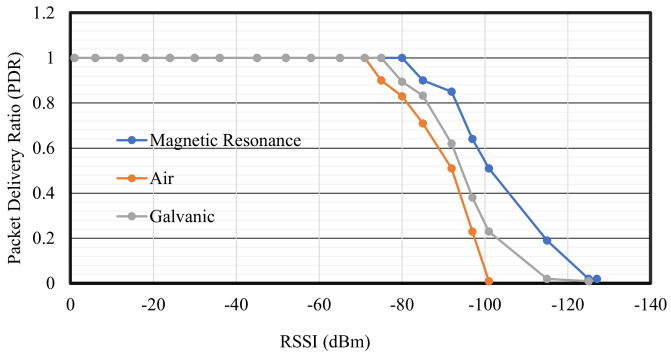

Fig. 8. Packet Delivery Ratio (PDR) versus RSSI

partly because much of the current flow in the case of galvanic coupling is local due to the way this technology works. It is also worth noticing that with MR, there is almost no packet drop for up to 65 cm distance, which would be plenty for most intra-body network applications. With a few potential retransmissions of lost packets, it is possible to stretch the communication range to almost 100 cm, where 50% of the packets are lost. As stated above, these results are for 1 mW of transmitted signal – in intra-body applications, it would be desirable to lower the power further to conserve the battery, which would reduce the range accordingly.

Fig. 8 illustrates the relationship between the packet delivery ratio (PDR) and received signal strength indicator (RSSI). It is seen to achieve 100% packet delivery, the RSSI can be down to -80 dBm for MR coupling but only -75 dBm for Galvanic coupling of the body. The corresponding number for air is -70 dBm. In a homogeneous medium, the PDR vs. RSSI generally does not depend on the media characteristics; however, this is not true for the body since it is a highly nonhomogeneous media as discussed earlier.

C. Packet Delivery Ratio vs. Packet Size

We conducted experiments to assess the packet delivery ratio (PDR) vs. the packet size as well, using MR coupling for human body. Fig. 9 shows the packet error rate (PER) (defined as 1-PDR), for air transmission of MR. The experiments used four different packet sizes (56,100,200, 300, and 400 Bytes). The received packets were identified as erroneous if they did not pass the 32-bit CRC as mentioned earlier. However, the much more significant reason for not receiving the packet is the error in the received preamble bits.

Any bit flip or unrecognized symbol in the preamble will miss the entire packet. (We ensured that the data in the packets did not contain the preamble pattern). As expected, the PER increases with the packet size, however, the increase is quite marginal from 56 bytes to 400 bytes. As surmised and extensively verified in [29], the errors in the preamble and data parts should be considered separately and could be quite different, with preamble error dominating the packet loss characteristics. This is exactly what Fig. 9 suggests. By assuming that the errors are independent at the bit level, and used two different bit error rates (BERs) for preamble and data (denoted p_p and p_d respectively), we can estimate the PER as a function of packet size. Here we did the opposite – we estimated p_p and p_d to best fit the observed PER, and then estimated PER as follows:

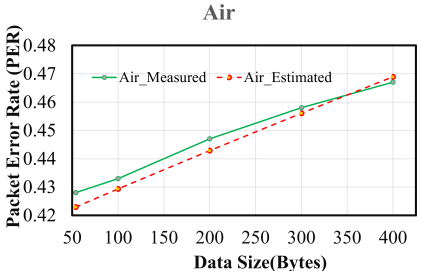

Fig. 9. Measured and Estimated PER vs. packet size in air media

$$PER_{\text{est}} = 1 - (1 - p_p)^{L_p}(1 - p_d)^{L_d} \quad (1)$$

where L_p and L_d are the lengths (in bits) of the preamble and data. In estimating p_p and p_d we made use of observed packets received with and without CRC errors; with preamble BER p_p considered independent of packet length. Fig. 9 also shows the estimated PER (with a dotted line). It is seen that the fit is excellent.

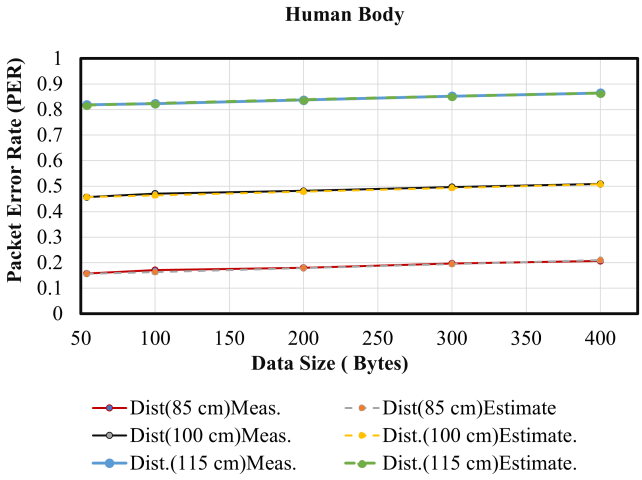

Fig. 10. Measured and Estimated PER vs. packet size in body media

Figure 10 shows similar data for the human body at 3 different distances, namely 85 cm, 100 cm, and 115 cm. These 3 distances were chosen to cover the estimated and measured PER for the human body versus the size of data in the different distances such as 85,100 and 115 cm were chosen based on Fig. 7 to cover different levels of delivery ratios. It is again

seen that the fit is excellent in all 3 cases. We observed that the estimated p_p and p_d both increase with distance, as expected; however, much of the change is in preamble BER (p_p); the data BER (p_d) changes much less significantly.

IV. Conclusions and Future Work

In this paper, we performed an experimental study of magnetic resonance (MR) coupling-based communication for use by on-body and intra-body nodes with the signal being communicated through the body. We showed that the mechanism works much better for transmission through the body than through the air. In particular, it is seen that at 1 mW transmitted power, the packets can be received without any error for up to 65 cm distance. At 50% packet loss, the range goes up to 100 cm, when needed, and a few retransmissions can easily communicate the packets reliably. We also compared MR transmission against galvanic coupling and showed that MR works significantly better.

We studied the packet error rate (PER) as a function of packet length and found that the error rate increases very slowly with the packet size. A simple error model, where all bits are assumed to be flipped independently, but the preamble BER is much higher than the data BER fits the experimental results extremely well. However, this does not necessarily validate the independence assumption. In the future, we will examine this issue further and accordingly explore how to improve the performance, including forwarding error correction.

Acknowledgement

The project was supported by the National Science Foundation (NSF) grants ECCS-2029077 (PI A. Kim), and CNS-1844944 (PI K. Kant). The authors would also like to acknowledge Olajide Q Yusuf from Temple University (Philadelphia, PA, USA) for his help with the experiments.

References

[1] L. P. Fried, "America's health and health care depend on preventing chronic disease," https://www.huffingtonpost.com/entry/americas-health-and-healthcare-depends-on-preventing_us_58c0649de4b070e55af9eade, March 2017.

[2] A. Tinker, "How to improve patient outcomes for chronic diseases and comorbidities," http://www.healthcatalyst.com/wp-content/uploads/2014/04/How-to-Improve-Patient-Outcomes.pdf, 2017.

[3] H. Y. Tung *et al.*, "The design of dual radio zigbee homecare gateway for remote patient monitoring," *IEEE Transactions on Consumer Electronics*, vol. 59, pp. 756–764, 2013.

[4] H. Tung *et al.*, "A mobility enabled inpatient monitoring system using a zigbee medical sensor network," *Sensors*, vol. 14, pp. 2397–2416, jan 2014.

[5] T. M. Bruns *et al.*, "Bursting stimulation of proximal urethral afferents improves bladder pressures and voiding," *Journal of neural engineering*, vol. 6, p. 066006, 2009.

[6] A. Mendez *et al.*, "Estimation of bladder volume from afferent neural activity," *IEEE Transactions on Neural Systems and Rehabilitation Engineering*, vol. 21, pp. 704–715, 2013.

[7] C. Powell, "Conditional electrical stimulation in animal and human models for neurogenic bladder: working toward a neuroprosthesis," *Current bladder dysfunction reports*, vol. 11, pp. 379–385, 2016.

[8] R. G. HAUSER, "Techniques for improving cardiac performance with implantable devices," *Pacing and Clinical Electrophysiology*, vol. 7, pp. 1234–1239, 1984.

[9] K. Kaszala *et al.*, "Device sensing: sensors and algorithms for pacemakers and implantable cardioverter defibrillators," *Circulation*, vol. 122, pp. 1328–1340, 2010.

[10] R. A. Normann *et al.*, "Clinical applications of penetrating neural interfaces and utah electrode array technologies," *Journal of neural engineering*, vol. 13, p. 061003, 2016.

[11] D. Werber *et al.*, "Investigation of RF transmission properties of human tissues," *Advances in Radio Science*, vol. 4, pp. 357–360, sep 2006.

[12] H.-Z. T. Chen *et al.*, "A study of rf power attenuation in bio-tissues," *Journal of Medical and Biological Engineering*, vol. 24, pp. 141–146, 2004.

[13] X. fang Li *et al.*, "Galvanic coupling type intra-body communication human body implantable sensor network," in *Advances in Intelligent and Soft Computing*. Springer Berlin Heidelberg, 2012, pp. 147–152.

[14] W. J. Tomlinson *et al.*, "Galvanic coupling intra-body communication link for real-time channel assessment," in *IEEE INFOCOM Workshops*, 2016.

[15] Y. Xu *et al.*, "Modeling and Characterization of Capacitive Coupling Intrabody Communication in an In-Vehicle Scenario," *Sensors*, vol. 19, p. 4305, oct 2019.

[16] A. Datta *et al.*, "Advanced biophysical model to capture channel variability for eqs capacitive hbc," *bioRxiv*, 2020.

[17] Y. K. Hernandez-Gomez *et al.*, "Magnetic human body communication based on double-inductor coupling," in *IEEE I2MTC*, vol. 9, 2017, pp. 1–6.

[18] T. Ogasawara *et al.*, "Human body communication based on magnetic coupling," *IEEE Transactions on Antennas and Propagation*, vol. 62, pp. 804–813, 2014.

[19] S. Banou *et al.*, "MAGIC: Magnetic Resonant Coupling for Intra-body Communication," in *IEEE INFOCOM*, vol. 2020-July, 2020, pp. 1549–1558.

[20] B. Kibret *et al.*, "Investigation of galvanic-coupled intrabody communication using the human body circuit model," *IEEE Journal of Biomedical and Health Informatics*, vol. 18, pp. 1196–1206, 2014.

[21] J. Park *et al.*, "Magnetic human body communication," in *IEEE EMBC*, 2015, pp. 1841–1844.

[22] N. Cho *et al.*, "The human body characteristics as a signal transmission medium for intrabody communication," *IEEE Transactions on Microwave Theory and Techniques*, vol. 55, pp. 1080–1086, 2007.

[23] T. G. Zimmerman, "Personal area networks: Near-field intrabody communication," *IBM Systems Journal*, vol. 35, pp. 609–617, 1996.

[24] U. S. R. Peripheral, "Universal software radio peripheral," http://www.ettus.com/, accessed: Aug 2021.

[25] R. University, "Warp: Wireless open-access research platform," hhttp://warpproject.or, accessed: Aug 2021.

[26] M. Bailleul, "Shielding of the electromagnetic field of a coplanar waveguide by a metal film: Implications for broadband ferromagnetic resonance measurements," *Applied Physics Letters*, vol. 103, p. 192405, Nov. 2013. [Online]. Available: https://doi.org/10.1063/1.4829367

[27] S. Islam *et al.*, "Performance evaluation of magnetic resonance coupling method for intra-body network," July 2021, available at https://www.kkant.net/vita_new.htm.

[28] "Guidelines for limiting exposure to time-varying electric and magnetic fields (1 Hz TO 100 kHz)," International Commission on Non-Ionizing Radiation Protection, Tech. Rep. 6, 2010.

[29] M. Jacobsson *et al.*, "Estimating packet delivery ratio for arbitrary packet sizes over wireless links," *IEEE Communications Letters*, vol. 19, pp. 609–612, 2015.